Dissipative features of the Vlasov equation in a simple model

1995 J. Phys. A: Math. Gen. 28 787

(http://iopscience.iop.org/0305-4470/28/4/008)

J. Phys. A: Math. Gen. 28 (1995) 787–803. Printed in the UK

Dissipative features of the Vlasov equation in a simple model

P L'Eplattenier†, E Suraud† and P G Reinhard‡

† Groupe de Physique Théorique, Laboratoire de Physique Quantique, Université Paul Sabatier, 118 Route de Narbonne, 31062 Toulouse cedex, France

‡ Institut für Theoretische Physik, Universität Erlangen, Staudtstrasse 7, D-91058 Erlangen, Germany

Received 25 January 1994, in final form 1 August 1994

Abstract. The dissipative properties of the Vlasov equation are investigated for a model system of A fermions in a harmonic oscillator plus a two-body interaction. The dissipation is quantified in terms of relaxation rates towards the final equilibrium which is a Boltzmann distribution in phase space. We look particularly for the dependence on the initial state and on the strength of the two-body interaction.

1. Introduction

Hamiltonian dynamics with a large number of degrees of freedom is a basic problem in many areas of physics. Rapidly growing computing power now permits large-scale simulations which allow deeper insight into the dynamical features of many-body systems [1]. One of the first investigations of this kind was the test of the ergodic hypothesis in the famous numerical experiment by Fermi *et al* [2]. They used a simplified Hamiltonian to allow a thorough computation of the full dynamics. The study of realistic systems, in particular, quantum or semi-classical systems, on the other hand, still requires some reduction in the description of the problem.

The lowest, and first, level of description is usually given by the Vlasov equation which constitutes the (semi-)classical mean-field description for the dynamics of the one-body distribution function. The Vlasov equation is widely used in various fields of physics such as gravitation [3], plasmas [4], semiconductors [5], and more recently nuclear physics [6]. The next higher level of description accounts for intermediate two-body collisions thus adding a collision term to the Vlasov equation. This leads to the Vlasov–Boltzmann equation for classical systems, such as, for example, a classical plasma [4]. Quantum systems of fermions require the Vlasov–Uehling–Uhlenbeck (VUU) equation whose collision term takes into account the Pauli blocking after the collision [6].

In three-dimensional problems, the Vlasov equation is commonly solved numerically by the so-called test-particle method. The idea of this method is to represent the one-body distribution function by a swarm of N numerical particles, the test particles, evolving in phase space. It can be shown that this evolution can be reformulated as an N-body Hamiltonian dynamics, which depends on the original physical A-body Hamiltonian and of the numerical parameters of the test-particle representation [7].

It has been pointed out in a previous publication that the actual solution of the Vlasov equation with the test-particle method displays dissipative features converging eventually to

0305-4470/95/040787+17$19.50

a stable equilibrium state which is given by the classical Boltzmann equilibrium distribution [7]. This causes problems for dense systems of fermions because the Boltzmann distribution can violate the Pauli principle allowing more than one identical fermion in one phase-space cell. One usually hopes to cure this problem by adding the Uehling–Uhlenbeck collision term which, as such, drives convergence towards a Fermi distribution. But it has been found in [7] that the drive towards a Boltzmann equilibrium, coming from the Vlasov equation, is competitive in strength such that the final VUU state is a mix between Fermi and Boltzmann equilibrium which violates the Pauli principle.

The purpose of this paper is to continue and to complement the previous investigations of [7]. We want to study now, in detail, the dependence of the dissipation on the initial state and on the strength of the residual two-body interaction, the model studied here allows us to tune the amount of nonlinearity through the self-consistent field, which was not possible in [7]. We thus consider a simple test case consisting of A fermions in an external oscillator potential and coupled via a purely two-body interaction. This model has several advantages for the present purposes. First, the predominance of the external field allows a systematic variation of the initial state without having the danger of a sudden and dramatic change of its internal structure. In other words, such a model allows a systematic check of the quality of the numerical initial condition, namely its closeness to the actual Thomas–Fermi ground state. Second, there is one pure two-body interaction (and no further, involved density dependence) which represents a clean and well controllable source for the residual interaction. And third, the simplicity makes the test case sufficiently general to be applicable to various fields of physics. We cite possible applications to nuclear and atomic physics but one could equally consider electronic transport in semiconductors or plasma physics.

The paper is organized as follows. In section 2, we briefly summarize some formal aspects of the Vlasov equation, the test-particle method, and the observables under consideration. And in section 3, we present and discuss the results.

2. Theoretical framework

2.1. The Vlasov equation and beyond

We consider a system of A interacting particles which is described by the A-body Hamiltonian

$$H = \sum_{i=1}^{A} \left(\tfrac{1}{2}p_i^2 + U_{\text{ext}}(r_i)\right) + \sum_{i<j} V(r_i - r_j)\,. \tag{1}$$

The particles move in an external one-body field U_{ext} and interact via the two-body potential V. The coordinates r and momenta p are three-dimensional vectors.

This paper concentrates on the widely used approximate treatment of the A-body dynamics in terms of the Vlasov equation

$$\frac{\partial f}{\partial t} + \{f, h(f, V)\} = 0 \tag{2}$$

with the self-consistent one-body (or mean-field) Hamilton operator

$$h(f, V) = \frac{p^2}{2m} + U_{\text{ext}}(r) + \int \mathrm{d}^3r'\, V(r, r') \underbrace{\int \mathrm{d}^3p\, f(r', p)}_{\rho(r')}\,. \tag{3}$$

This is a mean-field approach for A-body dynamics expressed in terms of $f(r, p)$, a hypothetical *smooth* one-body distribution in phase space, $\Gamma = (r, p)$. The Vlasov equation

emerges as the lowest-order approach of many-body hierarchies from different points of view.

For *classical* systems, the derivation starts from the Liouville equation in A-body phase space which is then recast into the BBGKY hierarchy of equations of motion for m-body subdensities [8]. Truncating the hierarchy at the lowest order, i.e. at the level of one-body densities, then yields the Vlasov equation (2). The next order correction can be constructed by considering the intermediate two-body collisions perturbatively. This extends the equation of motion to

$$\frac{\partial f}{\partial t} + \{f, h\} = \mathcal{I}_{\mathrm{B}}(f, V) \tag{4}$$

$$\mathcal{I}_{\mathrm{B}} = \alpha \int \mathrm{d}p_2\, \mathrm{d}p_3\, \mathrm{d}p_4\, |V|^2 \delta(E)\delta(p)[f(r, p_3)f(r, p_4) - f(r, p_1)f(r, p_2)] \tag{5}$$

where α is a constant and $\mathcal{I}_{\mathrm{B}}$ the Boltzmann collision term, $\delta(E)$ expresses energy conservation, and $\delta(p)$ momentum conservation over the collision. The collision term introduces dissipation into the dynamics such that the Vlasov–Boltzmann equations (4) and (5) drives the system towards a unique and stable equilibrium state which is described by the Boltzmann distribution

$$f_{\mathrm{B}} \propto \mathrm{e}^{-h/kT}\,. \tag{6}$$

Note that the determination of the equilibrium state constitutes a self-consistent problem because $h = h(f_{\mathrm{B}}, V_{12})$.

There is a very subtle problem involved in this derivation of the Vlasov(–Boltzmann) equation from the classical BBGKY hierarchy. The actual phase-space distribution of a system of A point particles is highly structured consisting out of sums of $\delta^6(\Gamma - \Gamma_i)$ distributions. This is not what the BBKGY hierarchy and the Vlasov equation are designed for. They imply a continuum limit where the particles are supposed to be sampled in cells in phase space and the phase-space distribution f stands for the smooth changes from one cell to another. There is a coarse-graining mechanism involved in between the original A-body problem and the final Vlasov(–Boltzmann) equation.

For *quantum* systems, one starts from the quantum many-body hierarchy and deduces as the lowest order a quantum mean-field dynamics, the time-dependent Hartree–Fock (TDHF) theory for the evolution of the one-body density operator $\hat{\rho}$ [9]. A phase-space representation of TDHF is achieved employing the Wigner transform [10]

$$A_{\mathrm{W}}(r, p) = \frac{1}{(2\pi\hbar)^3} \int \mathrm{d}q\, \mathrm{e}^{(\mathrm{i}/\hbar)p\cdot q} \langle r - q/2|A|r + q/2\rangle \tag{7}$$

for any one-body operator A. The TDHF equation in the Wigner representation then reads [11]

$$\frac{\partial \rho_{\mathrm{W}}}{\partial t} = -\frac{2}{\hbar} h_{\mathrm{W}} \sin\left(\frac{\hbar}{2}\left(\frac{\overleftarrow{\partial}}{\partial p}\frac{\overrightarrow{\partial}}{\partial r} - \frac{\overleftarrow{\partial}}{\partial r}\frac{\overrightarrow{\partial}}{\partial p}\right)\right)\rho_{\mathrm{W}} \tag{8}$$

where $\rho_{\mathrm{W}}(r, p)$ is the phase-space representation of the one-body density $\hat{\rho}$ and h_{W} the Wigner transformed mean-field Hamiltonian. A semiclassical expansion of that equation amounts to a Taylor expansion of the sine function in orders of $\hbar$. The Vlasov equation (2) then emerges as the lowest order of the expansion, i.e. in the classical limit $\hbar \longrightarrow 0$. Again one can derive the next order correction from a perturbative treatment of the intermediate two-body collisons. This yields the Vlasov–Uehling–Uhlenbeck (VUU) equation

$$\frac{\partial f}{\partial t} + \{f, h\} = \mathcal{I}_{\mathrm{UU}}(f, V_{12})\,. \tag{9}$$

The $\mathcal{I}_{UU}$ is the Uehling–Uhlenbeck collision term which is similar to the Boltzmann collision term (5) but with the blocking factors $f_3 f_4(1-f_1)(1-f_2)-(1-f_3)(1-f_4)f_1 f_2$ to account for the Pauli principle amongst fermions. Consequently, the Uehling–Uhlenbeck collision term $\mathcal{I}_{UU}$ drives towards a Fermi distribution

$$f_F = \frac{1}{1+\exp\left((h-\varepsilon_F)/kT\right)} \tag{10}$$

as the equilibrium stage, provided the Vlasov part of the VUU equation is indifferent to what the final equilibrium is. It is interesting to note that the fermionic nature of the particles shines through in the classical limit at the level of the collision term. The Pauli principle is a quantum effect which is not wiped out by the limit $\hbar \longrightarrow 0$. This would require a different limit, namely the limit of low density in phase space (e.g. at high temperatures).

Similarly to the classical derivation, there is a subtle problem with the supposed smoothness of the phase-space distribution f. The Wigner transformed quantum density ρ_W oscillates wildly [15]. Again one has to employ the concept of coarse-graining in phase space, e.g. by a Gaussian folding. This leads naturally to the Husimi picture which has been shown to deliver a more stable classical limit [16]. We will not dwell further on that very intricate detail and postpone it to a forthcoming publication.

There is a more practical problem with the VUU equation. Remember that the final Fermi equilibrum (10) is achieved by $\mathcal{I}_{UU}$ only if the Vlasov equation as such does not interfere. It is thus important to check the actual solution of the Vlasov dynamics for its own tendencies towards a final equilibrium stage. This has been done extensively in [7]. The result is that a test-particle solution of the Vlasov equation does indeed drive towards an equilibrium and this is the (classical) Boltzmann equilibrium (6), understandable because the Vlasov equation is a classical equation. This has the undesirable effect for long-time simulations with the VUU equation that the final equilibrium is an ill-defined mix between the Boltzmann and Fermi distribution, causing several side effects, such as the violation of the Pauli principle, or too high temperatures in the spectra of emitted particles. It is the aim of this paper to continue the investigation of the dissipative properties of the Vlasov equation with particular emphasis on the strength of the residual interaction and the initial excitation of the system.

2.2. *The test-particle method*

The standard way of simulating the Vlasov equation in high-dimensional problems is to use the test-particle method. The idea of the test-particle method is to project the one-body distribution function f onto a swarm of N numerical particles, which means to solve the Vlasov equation on a subspace of the one-body distribution functions space, on which f is approximated by

$$f_{\Delta,N}(r,p) = \frac{A}{N}\sum_{i=1}^{N} g(\Gamma-\Gamma_i) \qquad g(\Gamma-\Gamma_i) = g_r(r-r_i)g_p(p-p_i) \tag{11}$$

where here we use Gaussian sampling

$$g_r(r) = \left(\frac{2\sigma^2}{\pi}\right)^{3/2} \mathrm{e}^{-r^2/2\sigma^2} \qquad g_p(p) = \left(\frac{2}{\pi\sigma^2}\right)^{3/2} \mathrm{e}^{-\sigma^2 p^2/2}. \tag{12}$$

This is supposed to mock up the assumed smoothness of the one-body distribution (section 2.1). The momentum sampling is unimportant for the Vlasov equation because

$E_{kin} = p^2/2m$ commutes with the folding (except for a constant offset of zero-point energy). The sampling in coordinate space is relevant for accumulating the local density

$$\rho_g(r) = \frac{A}{N} \sum_i g_r(r - r_i) . \tag{13}$$

Many solution techniques employ an interpolating grid in coordinate space. The most stable representation is achieved when the folding width σ is related to the mesh size Δ of the coordinate-space grid by

$$\Delta = \sqrt{2 \log (2)} \sigma . \tag{14}$$

A distribution of point particles is recovered in the limit $\Delta \longrightarrow 0$. The approximately smooth distribution (11) can be expressed through the point distribution through a folding

$$f_{\Delta,N} = g \star f_{0,N} \qquad f_{0,N} = \frac{A}{N} \sum_{i=1}^{N} \delta^3(r - r_i) \delta^3(p - p_i) \tag{15}$$

where $\star$ stands for the folding operation.

The dynamics of the phase-space distribution f is then reduced to the dynamics of the test particles. Their equations of motion are obtained by minimizing an action on the r_i's and the p_i's:

$$S = \int \mathrm{d}t \left[\int \mathrm{d}r \, \mathrm{d}p \frac{p^2}{2m} f_{\Delta,N}(r, p) - \tfrac{1}{2} \int \mathrm{d}r \, \mathrm{d}p \, \mathrm{d}p' \mathrm{d}r' \, V_{12}(r - r') f_{\Delta,N}(r, p) f_{\Delta,N}(r', p') \right] \tag{16}$$

and read

$$\dot{r} = \frac{p}{m} \qquad \dot{p} = -\nabla (g \star h(f_{\Delta,N}, V)) . \tag{17}$$

Note that the folding g is used twice: first, when accumulating the density (13) to compute the self-consistent mean field, and second, when retriveing the force from the grid. Equations (17) actually appear as dynamical equations for N classical point particles corresponding to an effective N-body Hamiltonian

$$H_{\mathrm{eff}} = \sum_{i=1}^{N} \left(\frac{p_i^2}{2m} + U_{\mathrm{ext}}(r_i) \right) + \sum_{i<j} \frac{A}{N} (g \star V \star g)(r_i - r_j) . \tag{18}$$

(This Hamiltonian neglects the folding of U_{ext} which is approximately valid for soft external potentials and even exact for harmonic potentials.) The equations of motion (17) are solved numerically with the well known leap-frog algorithm [18].

The dissipative features of the test-particle dynamics can be estimated by again applying the BBGKY hierarchy to this effective N-body dynamics. This allows us to deduce that the test-particle method approximately corresponds to the dynamics [7]

$$\frac{\partial f}{\partial t} + \{f, h(f, V_{\mathrm{eff}})\} = \frac{A}{N} \mathcal{I}_{\mathrm{B}}(f, V_{\mathrm{eff}}) \qquad V_{\mathrm{eff}} = g \star V \star g . \tag{19}$$

This differs from the desired Vlasov equation (2) by the occurence of the Boltzmann collision term, which is suppressed by the factor A/N, and by the fact that the effective interaction V_{eff} is employed, which differs from V by a double folding. Thus *two* limiting processes are needed to recover the Vlasov dynamics: first, $N/A \longrightarrow \infty$ to suppress the collision term; and second, $\Delta \longrightarrow 0$ to explore the true interaction, i.e. $g \star V \star g \longrightarrow V$. The behaviour in the limit $N/A \longrightarrow \infty$ is well controlled. The other limit, $\Delta \longrightarrow 0$, is more involved. The folding of V corresponds to a suppression of the high Fourier components in V. A large

Δ thus dramatically reduces the effective cross section in the collision term. Lowering Δ enhances the cross section and much larger N/A are required to achieve sufficient reduction again. Thus the double limit is hard to establish in practice, in particular, if short-range interactions appear in the Hamiltonian [13].

It is then obvious from (19) that the test-particle method introduces artificial two-body dissipation which should scale as $(A/N)^1$. One also experiences a certain amount of one-body dissipation due to the reduction of information by sampling the density and the force, related to the fact that any finite representation has only finite resolution. This aspect is better seen in a different way of rewriting the test-particle dynamics. Inserting the equations of motion (17) for the test particles in the test-particle representation (11) for $\dot{f}$ and rewriting it in terms of Poisson brackets yields $\dot{f}_{\Delta,N} + \{f_{\Delta,N}, h(f_{\Delta,N}, V \star g)\} = 0$. Extracting the mismatch j with the desired Vlasov equation yields

$$\dot{f}_{\Delta,N} + \{f_{\Delta,N}, h(f_{\Delta,N}, V)\} = j \qquad j = \{f_{\Delta,N}, h(f_{\Delta,N}, V - V \star g)\}. \tag{20}$$

Here we see a deviation j at the one-body level due to fact that the equation which is actually solved contains one more folding in the interaction. It is to be noted, however, that the pertubation j also embraces the two-body dissipation because the mismatch j could be used directly to generate a collision term.

Last but not least, we have to remember that to evaluate any observable means to look at the system with reduced information. This means, for example, that the time evolution of a one-body observable shows additional one-body dissipation from reduced observation. This can even have dynamical consequences. For example, the Uehling–Uhlenbeck collision term in the VUU equation requires the measurement of the actual one-body phase-space distribution f. But this is sampled with a folding in phase space thus generating some one-body dissipation. In any case, we hesitate to disentangle further the dynamical and observational sources of one-body dissipation. It suffices to conclude that we have to expect both sorts of dissipation, two-body dissipation $\propto (A/N)^1$ and one-body dissipation $\propto (A/N)^0$, and that both have been indeed observed in practice [7]. An example of such a mix for the average relaxation times is given in (36).

2.3. The test case

In this paper, we consider a well controllable test case consisting out of a harmonic external field plus pure two-body force

$$U_{\text{ext}} = \tfrac{1}{2}r^2 \qquad V = c\delta^3(r - r') \qquad m = 1. \tag{21}$$

The external potential establishes proper binding under all circumstances and the parameter c provides a clean measure of the residual interaction. The string constant of the external oscillator is set to 1 as well as the mass of the physical particles. This means that we are working in natural units where the energy scale is set by the oscillator frequency ω and the length scale by the oscillator width $\sqrt{\hbar/m\omega}$. We use these natural units because the present model can serve as a schematic model in various different areas of physics. One merely has to replace the natural units by the typical scales of the problem.

For example, to view the results from a nuclear physics perspective, we introduce a mass $mc^2 = 940$ MeV for the nucleons and an oscillator frequency of $\omega = 0.05\ c$ fm^{-1} equivalent to $\hbar\omega = 10$ MeV. This yields the following scale factors:

length:	5.8 fm
time:	20 fm c^{-1}
energy:	10 MeV
coupling c:	1.5×10^4 MeV fm^3.

A typical atomic system would employ the electron mass $mc^2 = 0.5$ MeV and a frequency in the eV range which would lead to the following scale factors:

length:	2.8 Å
time:	0.6×10^{-15} s
energy:	1.0 eV
coupling c:	1.5×10^{-5} eV Å^3.

Here we aim to investigate specifically the effects of varying initial conditions and varying strengths of residual interaction. We thus avoid variation of particle number and folding width, which have been discussed extensively before, and take a standard test case with

$$A = 32 \qquad N = 2000 \qquad \sigma = 0.087 \tag{22}$$

where the folding width is given in natural units. Occasionally we will also vary the number of test particles, N/A, and it will be clearly indicated, but the two major quantities possibly varying will be the coupling strength c and the initial excitation energy.

A first side result of our investigations can be quoted here already. The simple two-body force allows two different ways of sampling the forces on the test particles. First, the standard sampling via an interpolating grid in coordinate space. And second, a simulation with a direct two-body potential V_{eff}:

$$\begin{aligned} h &= \frac{p^2}{2m} + \tfrac{1}{2}r^2 + c\sum_j V_{\text{eff}}(r - r_j) \\ V_{\text{eff}}(r - r_j) &= g \star g \star \delta = \mathrm{e}^{-((r-r_j)/2\sigma)^2}/(2\sigma\sqrt{\pi})^3 \end{aligned} \tag{23}$$

can be used. The latter case hence reduces to a pure (classical) molecular dynamics approach with a two-body interaction. We have compared both ways for a variety of cases and found no visible difference in the results, provided the mesh size Δ and folding width σ are related to each other according to (14). This confirms the validity of the technique using an interpolating coordinate space grid. It is to be noted that the interpolating grid becomes much more efficient at large N because it scales with N^1, whereas the direct two-body interaction scales with N^2.

2.4. The initial condition

We want to study systems of fermions. The semiclassical ground state is defined by the Thomas–Fermi distribution

$$f = \nu_{\text{F}}\vartheta(\epsilon_{\text{F}} - h(f, V)) = \nu_{\text{F}}\vartheta\Big(\underbrace{\epsilon_{\text{F}} - U_{\text{ext}}(r) - \int \mathrm{d}^3r'\, V\rho}_{\mu(r)} - \frac{p^2}{2m}\Big) \tag{24}$$

where ν_{F} is the number of internal degrees of freedom. For example, electrons have two spins yielding $\nu_{\text{F}} = 2$, whereas nucleons have spin and isospin yielding $\nu_{\text{F}} = 4$. Here we use $\nu_{\text{F}} = 2$. The equation (24) is obviously a nonlinear equation for f to be solved iteratively. This iteration can be simplified by integrating out the momenta. This yields a simpler equation for the local density distribution

$$\rho(r) = \frac{\nu_{\text{F}}}{6\pi^2}(2m\mu(r))^{3/2} \tag{25}$$

where μ depends on $\rho(r)$ as given in (24). This equation also needs to be solved iteratively for $\rho(r)$ but only in three spatial dimensions. The full distribution is then constructed from

(24) using the $\mu(r)$ obtained from solving (25). The distribution of the test particles is obtained by Monte Carlo sampling the coordinates r_i according to the density $\rho(r)$ and the momenta p_i in a sphere of radius $\sqrt{2m\mu}$.

We also want to vary the internal excitation of the system with respect to the Thomas–Fermi ground state. This is done simply by a monopole scaling in momentum space

$$p_i \longrightarrow \mathrm{e}^{\delta} p_i \tag{26}$$

where δ is an appropriate scaling strength. As an alternative, we consider a quadrupole deformation in momentum space

$$px_i \rightarrow \mathrm{e}^{\delta} px_i \qquad py_i \rightarrow \mathrm{e}^{\delta} py_i \qquad pz_i \rightarrow \mathrm{e}^{-2\delta} pz_i \,. \tag{27}$$

2.5. *The observables*

We aim to study the relaxation of the one-body phase-space distribution towards an equilibrium. An equilibrium distribution is characterized by $\{f, h\} = 0$, and thus $f = f(h)$. We therefore look at the energy distribution $D(\epsilon)$ which is obtained from sampling the single-particle energies $\epsilon_i = p_i^2/2m + U_i$ of the test particles in energy bins. But this energy distribution $D(\epsilon)$ as such is not yet very instructive because it is weighted with the single-particle level density $d(\varepsilon)$ in phase space which is defined by

$$d(\epsilon) = \nu_{\mathrm{F}} \int \mathrm{d}^6\Gamma \, \delta(h - \epsilon) = \nu_{\mathrm{F}} \frac{1}{4\pi^2} \int \mathrm{d}^3 r \left(\frac{2m}{\hbar^2}\right)^{3/2} (\epsilon - U(r))^{1/2} \tag{28}$$

and computed by direct numerical integration on the three-dimensional coordinate-space grid. We can then deduce the desired energy occupation

$$n(\epsilon) = D(\epsilon)/d(\epsilon) \,. \tag{29}$$

The questions are then whether the energy occupation relaxes towards an equilibrium, at which rate the relaxation takes place, and to which final distribution. The Boltzmann equilibrium (6) corresponds to

$$n_{\mathrm{B}} = \mathrm{e}^{(\varepsilon - \varepsilon_{\mathrm{B}})/kT_{\mathrm{B}}} \tag{30}$$

and the Fermi equilibrium (10) to

$$n_{\mathrm{F}} = \frac{1}{1 + \exp\left((\varepsilon - \varepsilon_{\mathrm{F}})/kT_{\mathrm{F}}\right)} \,. \tag{31}$$

In order to visualize the closeness to one of these two equilibria, we construct at any instant of time the energy-equivalent Boltzmann and Fermi distributions by adjusting $\varepsilon_{\mathrm{B/F}}$ and $T_{\mathrm{B/F}}$ to give the right number of particles and the right single-particle energy:

$$\langle n_{\mathrm{B/F}} \rangle = \langle n \rangle \qquad \langle \varepsilon n_{\mathrm{B/F}} \rangle = \langle \varepsilon n \rangle \tag{32}$$

where

$$\langle \alpha \rangle = \int \alpha(\epsilon) d(\epsilon) \, \mathrm{d}\epsilon \,. \tag{33}$$

The energy occupation $n(\varepsilon)$ is already a quite useful way to deliver compressed information on the state of the system, particularly if compared with the Boltzmann and Fermi equivalent distributions $n_{\mathrm{B/F}}$. But it is desirable to have one single number to characterize the closeness to the Boltzmann or Fermi equilibrium. This is provided by the entropy of the energy distribution

$$S = \int \mathrm{d}\varepsilon \, d(\varepsilon) \, n(\varepsilon) \log\left(n(\varepsilon)\right) \,. \tag{34}$$

This is then to be compared with the analogous entropy $S_{B/F}$ of the Boltzmann and Fermi equivalent distributions $n_{B/F}$. The usual outcome is that the Vlasov propagation in the test-particle method approaches $S \longrightarrow \lessapprox S_B$ [7] and we will confirm this for all cases considered here.

Furthermore, we are interested in a quantitative measure of the relaxation. To this end we fit the time evolution of the entropy, $S(t)$, to an exponential

$$S = S_\infty + a\,e^{-t/\tau}. \tag{35}$$

Those fits were achieved by a least-square method, giving a relaxation time τ. The error bar on τ is obtained by allowing variations of the χ^2 in a range of 20% above its minimal value.

3. Results and discussion

3.1. The initial condition

One of the aims of this paper is to investigate the stability of the initial Thomas–Fermi condition in connection with the numerical propagation of the Vlasov equation. For this task, it is important that the initial state is prepared with high quality. We thus will first check the properties of the initial state in this subsection. The considerations employ the standard test case as given in (22) and the coupling strength $c = 0.0035$. The initial state starts from a solution of the Thomas–Fermi equation (24) on the coordinate-space grid. This Thomas–Fermi ground state is then sampled with the test particles. It remains to be checked how well this sampling reproduces the ground state. Global properties, as energies and radii, are reproduced very well. This is demonstrated in table 1, where we compare the three parts of the total energy.

Table 1. Comparison of the Thomas–Fermi ground state on the grid with the test-particle sampling for different contributions to the energy, as indicated.

	Energies		
	Harmonic	Kinetic	Coupling
On the grid	58.00	51.92	4.00
Sampled	58.16	52.08	4.08

A more detailed observable is the energy occupation $n(\epsilon)$, as defined in section 2.5. The initial $n(\epsilon)$ computed from the test-particle ensemble is shown in figure 1. The result from the test-particle sampling with $N = 2000$ is a very good approximation to the constant value 1 inside the occupied states. The cut off at the Fermi energy ϵ_F looks a bit softer than the required $\vartheta(\epsilon_F - \epsilon)$. But remember that the energy occupation is sampled in energy bins of 0.6 natural units. The width of the sampled $n(\epsilon)$ is just somewhat larger than the distance of these bins. This means that we have reproduced the initial $\vartheta(\epsilon_F - \epsilon)$ within the resolution of our sampling. The initial state is a fermionic state by construction, and this feature is confirmed by comparison with the equivalent Fermi occupation n_F. The corresponding Boltzmann occupation n_B is obviously far away from this initial state.

The initial local density $\rho(r)$ is shown in figure 2. The result from the test-particle ensemble can be considered as a good approximation to the original density on the grid. (Remember that the density from the test-particle representation is sampled on radial bins of 0.08 natural units.)

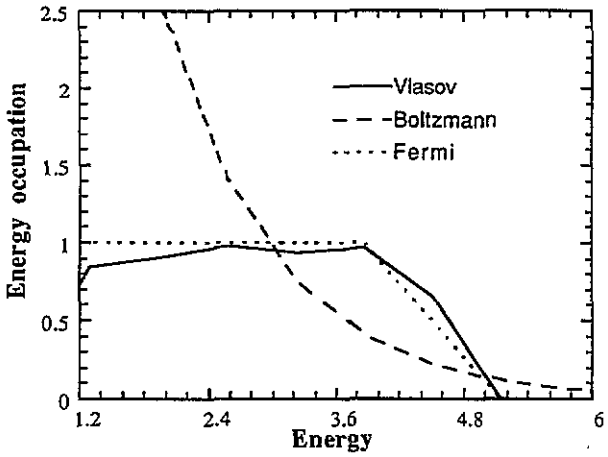

Figure 1. Energy occupation $n(\epsilon)$ of the initial Thomas–Fermi ground state in test-particle representation (full curve). The equivalent Fermi (dotted) and Boltzmann occupations (broken) are shown for comparison. The minimum energy is above 0 due to the mean field from the repulsive interaction.

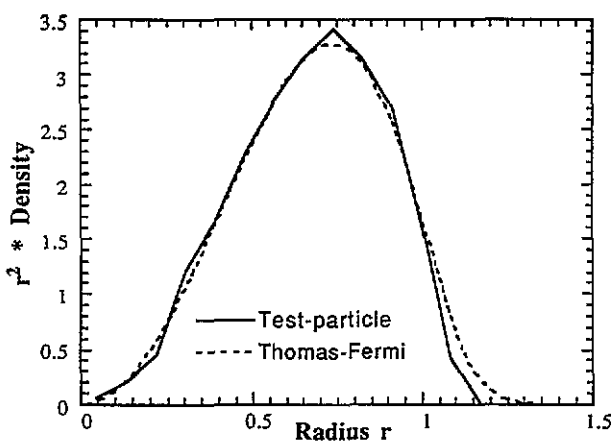

Figure 2. Radial local density distribution $\rho(r)$ weighted with r^2 for the initial state from the test-particle representation (full curve) and from the Thomas–Fermi solution on the grid.

3.2. Analysis of the time evolution

This section shows that the Vlasov dynamics drives a system away from the Fermi equilibrium towards a Boltzmann equilibrium [7]. The new aspect here is that we now start from the Thomas–Fermi ground state which is supposed to be a stationary state of the Vlasov equation. And yet the result is exactly the same as before: the system is unstable in the initial state, which obeys the Pauli principle, and relaxes towards a final Boltzmann equilibrium. Furthermore, this section serves to demonstrate the various ways of looking at this relaxation process for one typical example.

We have seen in the previous subsection that the initial condition nicely establishes a Fermi distribution. But the Vlasov dynamics of the system quickly explores the fact that this distribution is not a stable equilibrium state. It drives the system away from the initial state and converges towards the stable equilibrium of a classical system

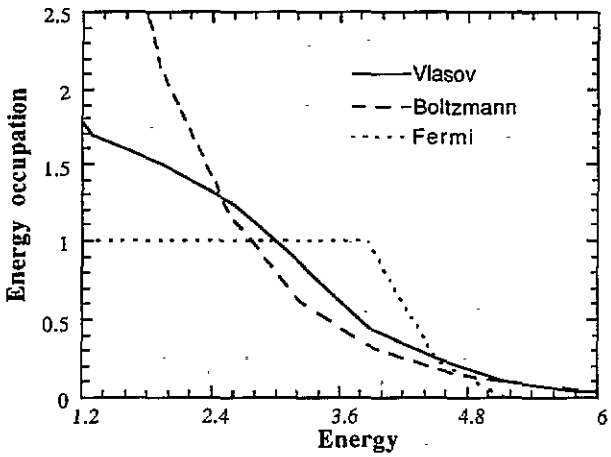

Figure 3. *Energy occupation $n(\epsilon)$ for the standard test case with $c = 0.0035$ at $t = 150$* natural units. a late stage of the time evolution. The equivalent Fermi (dotted) and Boltzmann occupations (broken) are shown for comparison.

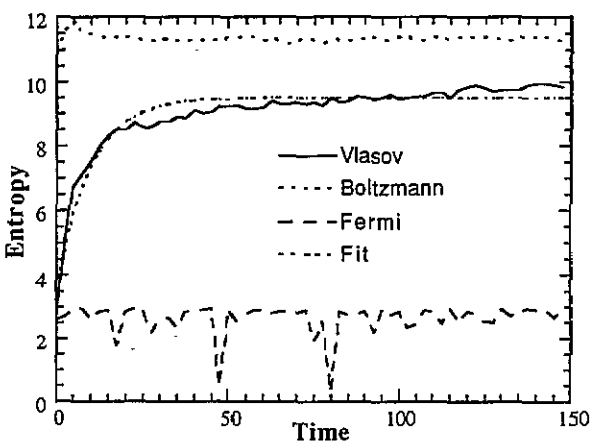

Figure 4. The entropy S of the energy occupation (full curve) versus time, compared with the Fermi and Boltzmann equivalent entropies S_F (long broken) and S_B (short broken), and, furthermore, compared with a relaxation ansatz (dotted) whose relaxation time is $\tau = 12.43$, which is to compare with the period of the external harmonic oscillator $T = 6.28$.

which is the Boltzmann distribution. This is demonstrated in figure 3, where we show the energy occupation after propagating the initial state of the previous subsection for 150 time units. It is obvious that the distribution has moved far away from a Fermi distribution. It is very close to a Boltzmann distribution. The remaining deviations from the equivalent Boltzmann distribution are due to dynamical fluctuations (effectively Langevin fluctuations). They change their shape quickly from one snapshoot to the next. But they never disappear.

The full energy occupation $n(\epsilon)$ is quite instructive. But it is very cumbersome to trace changing pattern during time evolution. Therefore, the energy occupation is characterized by one number, the entropy S as defined in (34). Analogously, there are the entropies S_F and S_B of the equivalent Fermi and Boltzmann distributions. We show in figure 4 these

entropies as function of time for the standard test case of this and the previous section. One clearly sees the instability of the inital Fermi equilibrium and the convergence towards a final Boltzmann distribution. The actual entropy S is bound to stay below S_B at all times because it contains Langevin fluctuations and these fluctuations always act to lower the entropy [7].

The pattern of $S(t)$ is already a quite compressed information on the dynamics. Nonetheless, it can become cumbersome to look at a large variety of these data if one wants to trace down trends. As seen in figure 4, one can characterize the $S(t)$ very well by exponential relaxations (35).

The value of the relaxation time obtained in this standard case is $\tau \approx 12.4$, which is about three times the period of the harmonic oscillator $\tau = 2\pi/\omega = 6.28$. This clearly shows the importance of the relaxation process studied in this paper, which takes place in a time-scale comparable to characteristic time-scales of the system.

3.3. Variation of the initial energy

We have seen in [7] that an excited system converges towards a Boltzmann equilibrium, and we have confirmed in the previous subsection that a system starting in a Thomas–Fermi ground state does the same. There remains the question of how the observed relaxation times depend on the internal excitation of the initial state. The simplicity of the one-body Hamiltonian choosen here allows a clear investigation of close to ground state cases. One can hence study the stability at low excitation of the system. We show in figure 5 the relaxation rates for systematically varied excitation energies using the two different excitation mechanisms outlined in section 2.4. In this regime of small excitation, the scaling mainly enhances the initial value of the entropy (which provides an indicator of the closeness of the true ground state) but the relaxation process remains essentially independent of the excitation energy. The result is not surprising if we look at it from the appropriate reference point. The excitation energy in figure 5 was measured with respect to the Thomas–Fermi ground state, and thus the change from zero energy to any

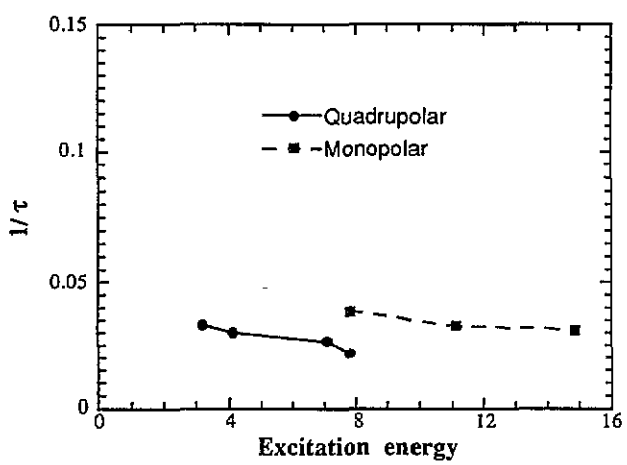

Figure 5. The average relaxation rate $1/\tau$ versus internal excitation energy (measured with respect to the Thomas–Fermi ground state) for various types of initial excitation: monopole scaling of momenta (full squares connected by a broken line) and quadrupole scaling of momenta (full circles connected by a full line).

excitation looks huge. The true equilibrium, however, is the classical Boltzmann equilibrium which is far below the Thomas–Fermi ground state and thus has a high temperature when starting from anything above this Thomas–Fermi 'ground state'. The variations relative to the Boltzmann equilibrium state are much smaller. The Boltzmann temperatures of the final states in figure 5 vary only between $kT = 1.030$ and 1.041, which is not such a dramatic variation. Thus the small changes in the observed relaxation are indeed very plausible.

3.4. Variation of the coupling

The present model (21) is designed to contain only one interaction which is a pure two-body force. This is then the unique and density-independent residual interaction which acts as the source for the observed dissipation. The confining oscillator potential provides a fairly constant spatial extension of the system such that we have a clean separation of the interaction effects parametrized through c, the strength of the two-body interaction.

Figure 6 shows the entropies $S(t)$ for systematically varied coupling strength c. One sees nicely how the relaxation slows down with decreasing coupling c. The Langevin fluctuations are also related to the dissipation, i.e. they are large where the relaxation rate is high and vice versa.

The corresponding average relaxation times and their uncertainties are shown in figure 7. This figure suggests that the relaxation rate depends linearly on c. There remains, however, a faint problem concerning the fact that the two-body interaction also modifies the one-body mean field through the self-consistent contribution $c \int d^3r' \delta(r - r')\rho(r')$. In order to quantify this side-effect, we change the curvature of the external oscillator, $\frac{1}{2}r^2 \longrightarrow \frac{1}{2}ar^2$, such that the total curvature of the effective mean field (including the $c \int d^3r' \delta(r - r')\rho(r')$ term) is kept constant. This readjustment is done for the curvature near $r = 0$. It turns out that this readjustment of the effective mean field is perfect in the region of interest where $\rho(r) \neq 0$. The results of this variant are also indicated with stars in figure 7. They coincide with the previous results which demonstrates that the relevant parameter governing the dissipation is c, the strength of the two-body interaction.

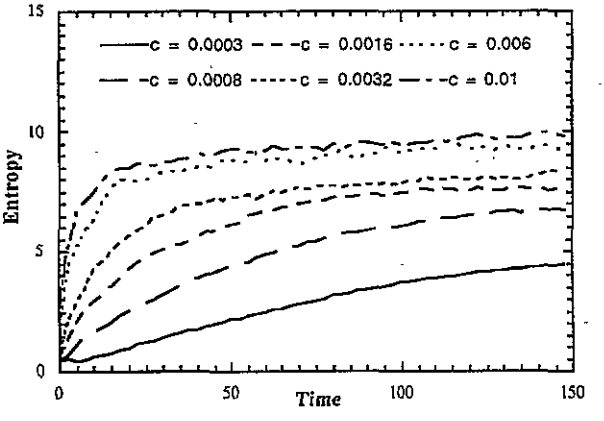

Figure 6. The entropy S of the energy occupation versus time for various strengths of the coupling constant c as indicated (in natural units).

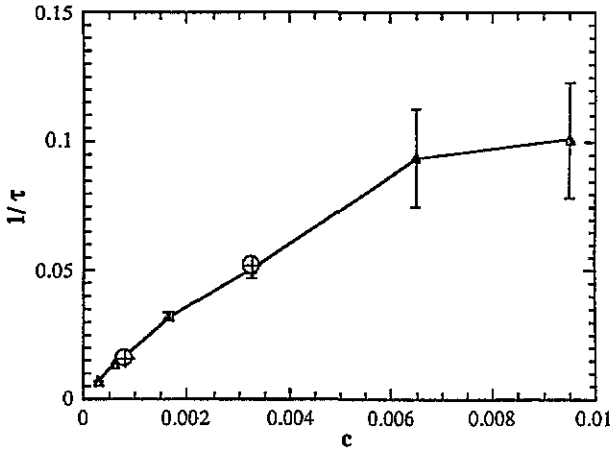

Figure 7. The average relaxation rates $1/\tau$ versus coupling strength c (both in natural units). The error bars indicate the estimated uncertainty on $1/\tau$. The open triangles connected by the full line are results from the standard model. The crossed circles are results from a variant of the model where the curvature of the external potential has been reajusted to minimize the effect of the self-consistent potential.

3.5. Separation of one- and two-body dissipation

The linear relation between $1/\tau$ and c, as observed in figure 7, seems at first glance natural. But at a second thought, one would rather have expected a dependence like c^2 because the collisions count in that order. The point is that we have to distinguish between one-body and two-body dissipation. The two-body dissipation is related to collisions of the test particles. It can be described by a Boltzmann collision term which has a cross section $\sigma \propto |V_{12}|^2 \propto c^2(A/N)$, as can be deduced from (5) and (19). The relaxation rate is then $1/\tau \propto \sigma$. The one-body dissipation comes from the finite resolution and the finite sampling of the one-body density, and subsequently of the one-body potential. It is thus independent of the number of test particles, $\propto (A/N)^0$, and linear in c as the mean field $c\rho$. Therefore, it was suspected in [7] that both dependences should occur, yielding a mix

$$\frac{1}{\tau} = \alpha_1 \frac{1}{\tau^{(1)}} c^1 \left(\frac{A}{N}\right)^0 + \alpha_2 \frac{1}{\tau^{(2)}} c^2 \left(\frac{A}{N}\right)^1 \tag{36}$$

of one-body dissipation ($\propto c^1$) and two-body dissipation ($\propto c^2$). The accuracy of our numerical treatment and the simple form of the residual interaction allows us to explore this distinction in more detail. The data in figure 7 suggest a predominance of one-body dissipation. This can be counterchecked by drawing the relaxation rate versus A/N, as is done for three values of c in figure 8. Remember that our standard test case used $A/N = 0.016$. The offset at $A/N \to 0$ displays the one-body dissipation term $\propto (A/N)^0$, whereas the slope gives a hint on the two-body dissipation $\propto (A/N)^1$. Figure 8 shows clearly that one-body dissipation is dominant in the present model for the range of A/N which we have used.

The curve in figure 8 corresponding to $c = 0.005$ shows two regimes. This is explained by the fact that this case already has a large amount of self-consistent feedback. As a consequence it becomes not so easy to produce a high-quality initial condition any longer. Taking the initial entropy as a critical check, we see that the initial state already shows strong fluctuations deviating from a Fermi distribution large A/N, i.e. for a small number

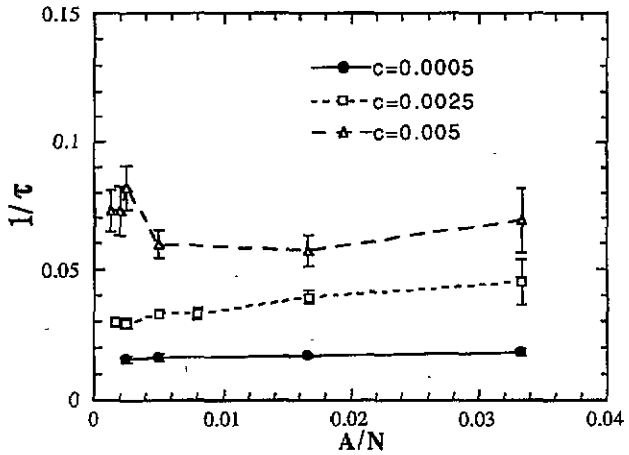

Figure 8. The average relaxation rates $1/\tau$ versus the inverse number of test particles A/N for three different coupling strengths c as indicated.

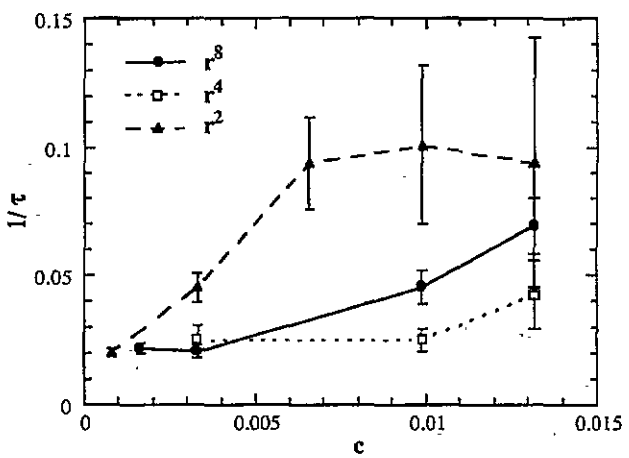

Figure 9. The average relaxation rates $1/\tau$ versus coupling strength c (both in natural units) for three different external potentials: $\propto r^2$, triangles connected by a long broken line; $\propto r^4$, square boxes connected by a short broken line; and $\propto r^8$, circles connected by a full line.

of test particles. A particularly high resolution is required for the stronger coupling; in practice we need typically $A/N \leqslant 0.0033$. Thus, in the $c = 0.005$ curve for large A/N, the system starts from an initial condition which already deviates from a Fermi distribution, and then it misses the initial fast relaxation, leading to a longer average relaxation time. This interpretation is confirmed by the fact that for small A/N, where the initial entropy is properly set, one again recovers an almost constant dependance on A/N. Altogether, the results of figure 8 taken at small A/N are consistent with the linear trend with c observed in figure 7. A further countercheck would be to evaluate the trend of the slopes in figure 8 relative to c^2 in order to disentangle the contribution from the two-body dissipation. However, the data in this figure are not sufficient for a conclusive answer.

3.6. Other external potentials

The test case of this paper employed the oscillator potential $\propto r^2$ as the external field. This is a very particular potential. We therefore want to countercheck the results for alternative external potentials. We choose the two further cases $U \propto r^4$ and $U \propto r^8$, both adjusted such that the RMS radius of the system is comparable to the oscillator case. Of course, the system also converges in these alternative cases towards a Boltzmann distribution. The question is at which rate. The relaxation rates for various coupling strengths c are compared in figure 9 for the three external potentials. For the three cases, $1/\tau$ roughly increases with the coupling constant c. The results differ in the details but the orders of magnitude of relaxation remain similar. From a qualitative point of view, it nevertheless does not seem that the detailed shape of the external potential has a critical influence on the dissipation. As expected, the dominant source of dissipation remains the residual two-body interaction.

4. Conclusion

We have investigated the dissipative aspects of the Vlasov dynamics in the test-particle solution, i.e. the fact that the state of the system develops towards a final equilibrium state which consists of a Boltzmann distribution and some Langevin fluctuations about it. The state of the system is visualized in terms of the energy occupation $n(\epsilon)$, the probability density with which a level at energy ϵ is occupied. The energy occupation indicates visually the structure of the level, whether it resembles more a Fermi distribution or a Boltzmann distribution. The typical shape of the energy distribution can be characterized by one number—the entropy in relation to the entropies of the equivalent Fermi and Boltzmann distributions. This allows us to draw conclusions on the relaxation times by watching the convergence of the entropy towards its equilibrium value in the course of the time evolution. Using these observables, we have particularly considered the effects of the initial state and of the residual interaction on the dissipation.

We have prepared a fermionic ground state of the system from the solution of the Thomas–Fermi equation. This state is a stationary state of the Vlasov equation. But it turns out to be an unstable equilibrium, where any small fluctuation triggers a quick deviation from the Thomas–Fermi state and steady relaxation towards the final Boltzmann equilibrium. We have varied the initial state by a systematic increase of excitation energy with respect to the Thomas–Fermi ground state. We find that the relaxation times are insensitive to this variation of the initial energy. The relaxation process proceeds very similarly in all cases, except perhaps for the first few time steps.

The simplicity of the test case, confining external field plus two-body interaction, allowed a well controlled variation of the strength of the residual interaction, in particular, in a perturbative regime. Variation of the external field has shown that the relaxation times depend predominantly on the residual interaction and very little on the external field. Variation of the strength of the residual interaction delivered a linear dependence of the relaxation rates (i.e. inverse relaxation times) on the coupling strength, hinting at a predominance of one-body dissipation for our test case. This has been confirmed by disentangling one- and two-body dissipation from a variation of the number of test particles. It is to be noted that previous investigations using a realistic nuclear interaction have shown more two- than one-body dissipation [7]. The relative weight of these two mechanisms thus depends on the actual Hamiltonian and needs to be checked anew in every case. In any case, there remains the strong relaxation towards the classical Boltzmann equilibrium whose rate competes with other relaxation processes, as, for example, the drive towards a

Fermi equilibrium from the fermionic Uehling–Uhlenbeck collision term. This unwanted competition causes serious doubts on the applicability of the Vlasov–Uehling–Uhlenbeck equation for long-time simulations of fermion dynamics. What one needs is a classical limit of the particle dynamics which preserves the memory on the fermionic nature of the particles involved.

References

[1] Hoover W G 1991 *Computational Statistical Mechanics* (New York: Elsevier)
[2] Fermi E, Pasta J and Ulam S 1965 *Collected Papers of E Fermi* vol 2, ed E Segre (Chicago, IL: University of Chicago) p 978
[3] Peebles P J E 1980 *The Large Scale Structure of the Universe* (Princeton, NJ: Princeton University Press)
[4] Vlasov A A 1950 *Many Particle Theory and its Applications to Plasma* (New York: Gordon and Breach)
[5] Brout R and Carruthers P 1963 *Lectures on the Many-Electron Problem* (New York: Wiley)
[6] Bertsch G F and Das Gupta S 1988 *Phys. Rep.* **160** 190
[7] Reinhard P-G and Suraud E1993 *Preprint* LPQTh 93-10 and 93-12 (submitted to *Ann. Phys., NY*)
[8] Balescu R 1975 *Nonequilibrium Statistical Mechanics* (New York: Wiley)
[9] Ring P and Schuck P 1980 *The Nuclear Many-Bo'dy Problem* (Heidelberg: Springer)
[10] Balaz N L and Jennings B K 1984 *Phys. Rep.* **104** 347
[11] Moyal J E 1949 *Proc. Camb. Philos. Soc.* **45** 99
[12] Takahashi K 1989 *Prog. Theor. Phys.* **98**
[13] Wong C Y 1982 *Phys. Rev.* C **25** 1460
[14] Reinhard P-G and Toepffer C 1994 *Int. J. Mod. Phys.* E to appear
[15] Takahashi K 1986 *J. Phys. Soc. Japan* **55** 762
[16] Takahashi K 1988 *J. Phys. Soc. Japan* **57** 442
[17] Vautherin D and Brink D 1972 *Phys. Rev.* C **5** 626
[18] Verlet L 1967 *Phys. Rev.* **159** 89